Epsilon-Near-Zero Substrate Engineering for Ultrathin-Film Perfect Absorbers

Jura Rensberg, You Zhou, Steffen Richter, Chenghao Wan, Shuyan Zhang, Philipp Schöppe, Rüdiger Schmidt-Grund, Shriram Ramanathan, Federico Capasso, Mikhail A. Kats, and Carsten Ronning

Epsilon-near-zero substrate engineering for ultra-thin-film perfect absorbers

Jura Rensberg[1], You Zhou[2], Steffen Richter[3], Chenghao Wan[4, 5], Shuyan Zhang[2], Philipp Schöppe[1], Rüdiger Schmidt-Grund[3], Shriram Ramanathan[6], Federico Capasso[2], Mikhail A. Kats[4, 5], Carsten Ronning[1]

[1]Institute for Solid State Physics, Friedrich-Schiller-Universität Jena, 07743 Jena, Germany

[2]John A. Paulson School of Engineering and Applied Sciences, Harvard University, Cambridge, MA 02138, USA.

[3]Institute for Experimental Physics II, Universität Leipzig, 04109 Leipzig, Germany

[4]Department of Materials Science and Engineering, University of Wisconsin - Madison, Madison, Wisconsin 53706, USA

[5]Department of Electrical and Computer Engineering, University of Wisconsin - Madison, Madison, Wisconsin 53706, USA

[6]School of Materials Engineering, Purdue University, West Lafayette, IN 47907, USA

Abstract

Efficient suppression of reflection is a key requirement for perfect absorption of light. Recently, it has been shown that reflection can be effectively suppressed utilizing a single ultra-thin film deposited on metals or polar materials featuring phonon resonances. The wavelength at which reflection can be fully suppressed is primarily determined by the nature of these substrates, and is pinned to particular values near plasma or phonon resonances – the former typically in the ultraviolet or visible, the latter in the infrared. Here, we explicitly identify the required optical properties of films and substrates for the design of absorbing anti-reflection coatings based on ultra-thin films. We find that completely suppressed reflection using films with thicknesses much smaller than the wavelength of light occurs within a spectral region where the real part of the refractive index of the substrate is $n \lesssim 1$, which is characteristic of materials with permittivity close to zero. We experimentally verify this condition by using an ultra-thin vanadium dioxide film with dynamically tunable optical properties on several epsilon-near-zero materials, including aluminum-doped zinc oxide. By tailoring the plasma frequency of the aluminum-doped zinc oxide, we were able to tune the epsilon-near-zero point, thus achieving suppressed reflection and near-perfect absorption at wavelengths that continuously span the near-infrared and long-wave mid-infrared ranges.

I. Introduction

Enhancing the absorption of light is of great importance for applications including photovoltaics[1-5], biosensing[6], light detection[7], thermal imaging[8-10], and efficient light emission[11-14]. Unfortunately, materials featuring large optical absorption coefficients tend to be highly reflecting, due to the large impedance mismatch at interfaces with air or other

transparent dielectrics, thus limiting the total amount of power absorbed. A well-known approach for suppressing interface reflections involves the use of single- and multi-layer dielectric anti-reflection (AR) coatings[15]; however, these AR coatings are typically at least a quarter-wavelength of light in thickness, which can become a limitation at longer wavelengths (e.g. in the mid and far infrared). Another approach involving gradient-index structures suffers from similar thickness limitations[16, 17].

An alternative approach to suppress undesired reflections involves "metamaterial" or "plasmonic" absorbers, which feature strong narrowband absorption resonances[8, 18-28]. This type of device typically consists of a metallic back reflector, a thin dielectric spacer, and periodically patterned subwavelength resonators on the front, and can achieve complete absorption resulting from critical coupling[29, 30]. Nevertheless, such absorbers typically require complex designs and the use of sophisticated lithography techniques, limiting their scalability to large areas.

Recently, it has been shown that near-perfect optical absorption can be achieved using ultra-thin lossy coatings on reflecting substrates, circumventing the "quarter-wavelength" lower limit on the thickness of unpatterned AR coatings[13, 31-39]. This effect is enabled by the nontrivial phase shifts at the film interfaces, which can be modified by varying the degree of loss (quantified by the extinction coefficient κ) in the film and substrate. These interface phase shifts contribute to the condition for destructive interference of the reflected light, which can then be achieved for thickness d much smaller than a quarter of the wavelength in the film.

Over the past years, several material combinations have been successfully used to achieve near-perfect absorption in ultra-thin absorbing coatings across the spectral range from visible to infrared. These include semiconductors like germanium (Ge), silicon (Si), and gallium arsenide, as well as metallic substrates like silver, gold and aluminum, suitable for applications in the visible[32,33,35,36,39]. For example Park et al.[35] demonstrated 98% absorption within a 12 nm thin Ge layer on top of a silver substrate at a wavelength of $\lambda = 625$ nm. Second, phase transition materials like vanadium dioxide, semiconductors and dielectrics on polar dielectric materials in their respective Reststrahlen band region are suitable for the mid-infrared and infrared spectral region[31,34]. Kats et al.[31] demonstrated near-perfect reflection and 90% absorption within a 180 nm vanadium dioxide (VO_2) thin film, which was deposited on a sapphire substrate, at a wavelength of 11.8 µm that corresponds to the Reststrahlen band of sapphire. And third, dielectrics on highly-doped semiconductors have been demonstrated for

applications in the mid-infrared[33]. As an example, Schlich et al.[33] used a 165 nm thin Ge coating, which is transparent in the mid-infrared, to almost completely suppress the reflection of light from a highly n-doped silicon substrate at 5.6 µm. The thickness of the Ge coating is about half the thickness of a conventional transparent AR coating on a comparable transparent substrate.

Despite numerous recent experimental demonstrations of enhanced light absorption in ultra-thin lossy films, the parameter space of possible substrate and film combinations has not been fully explored. Especially the spectral region not accessible with metallic and polar substrate materials has to be further explored. In this article, we introduce and experimentally verify a general strategy that facilitates the design of antireflection coatings and near-perfect absorbers based on ultra-thin films. We identified that suppressed reflection using films with thicknesses much smaller than the wavelength of light can only be achieved if the real part of the refractive index of the substrate n is $\lesssim 1$, which is most commonly found in the vicinity of phononic or plasmonic resonances, where a crossover of the real permittivity from positive to negative results in an epsilon-near-zero (ENZ) condition[40]. Here, we want to explicitly highlight the use of tunable ENZ materials, such as the transparent conductive oxides, that enable applications at near-infrared wavelength.

Our experimental verifications utilize subwavelength films of VO_2 grown on phononic and plasmonic substrates. The reversible insulator-to-metal transition in VO_2, often considered for optical switching[41-43], provides access to a broad range of complex refractive index values, especially in the mid-IR[44], allowing us to effectively perform multiple experiments using the same sample. For this reason, VO_2 has been used to demonstrate ultra-thin film absorbers in the past, using substrates such as sapphire[31, 45] and noble metals[38]. However, these substrate choices tie the wavelength of operation to particular narrow bands.

By adjusting the plasma frequency of aluminum doped zinc oxide (AZO), one of the most prominent ENZ materials[46-54], we demonstrate that the wavelength of suppressed reflection (and, thus, near-perfect absorption) can be arbitrarily selected within the near- and mid-infrared ranges.

II. Materials and methods

Aluminum-doped zinc oxide (AZO) substrates were fabricated using ion implantation. Undoped (001) zinc oxide (ZnO) single crystals were implanted at 500 °C with Al^+ ions with energies ranging from 30 to 350 keV, and various fluences, to achieve homogenous box-like

doping profiles that range 400 nm from the surface into the substrate with constant aluminum concentrations (c_{Al}) ranging from 1×10^{19} to 1×10^{21} cm^{-3} and a Gaussian doping tail that ranges additional 200 nm into the substrate (compare Appendix A). The high-temperature Al^{+} implantation was followed by thermal annealing in air for one hour at 700 °C. The annealing was necessary to reduce the number of lattice defects created by ion irradiation and to activate the majority of aluminum dopants. No long-range diffusion of Al dopants is expected at these temperatures[55, 56]. The optical properties of the ZnO and AZO substrates were determined by variable-angle spectroscopic ellipsometry (compare Appendix A).

VO$_2$ thin films were grown on (001) quartz (SiO$_2$), (001) ZnO, and the ion-implanted (001) AZO substrates. The films were grown using radio-frequency magnetron sputtering from a V$_2$O$_5$ target, with the temperature, pressure, and argon gas flow maintained at 450 °C, 5 mTorr, and 40 sccm, respectively. The same VO$_2$ growth recipe was used for all substrates, initially optimized for sapphire[57]. The resulting VO$_2$ film thickness was ~ 100 nm on ZnO and AZO, and ~ 200 nm on SiO$_2$.

The reflectance of each sample was investigated at near-normal incidence in the mid-IR, using a microscope (Bruker Hyperion 2000), attached to a Fourier transform infrared (FTIR) spectrometer (Bruker Vertex 70). All spectra were collected at temperatures between 30 °C and 100 °C with increment of 1 °C.
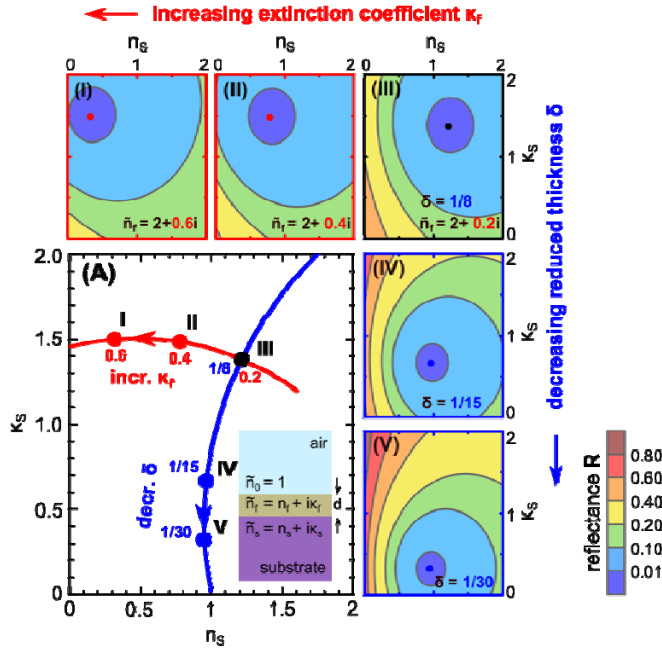
III. Results and discussion

A. Suppression of light reflection

To identify film/substrate combinations that yield zero reflection, we calculated the reflectance of an asymmetric Fabry-Perot-type structure [inset Fig. 1(A)] comprising a thin film with thickness d and refractive index $\tilde{n}_f = n_f + i\kappa_f$, sandwiched between air ($\tilde{n}_0 = 1$) and a substrate with refractive index $\tilde{n}_s = n_s + i\kappa_s$. We consider light incidence perpendicular to the surface from the air side. The reflectance is given by $R = |r|^2$ where:

$$r = \frac{r_{0,f} + r_{f,s}e^{2i\phi}}{1 + r_{0,f}r_{f,s}e^{2i\phi}}, \qquad (1)$$

and $r_{p,q} = (\tilde{n}_p - \tilde{n}_q)/(\tilde{n}_p + \tilde{n}_q)$ are the Fresnel reflection coefficients for normal incidence as the wave encounters medium q from medium p, $\tilde{n}_p$ and $\tilde{n}_q$ are the complex refractive indices of

medium p and q, respectively, and $\phi = \dfrac{2\pi}{\lambda} d\tilde{n}_f$ is the complex phase shift accumulated upon wave propagation within the film[58].
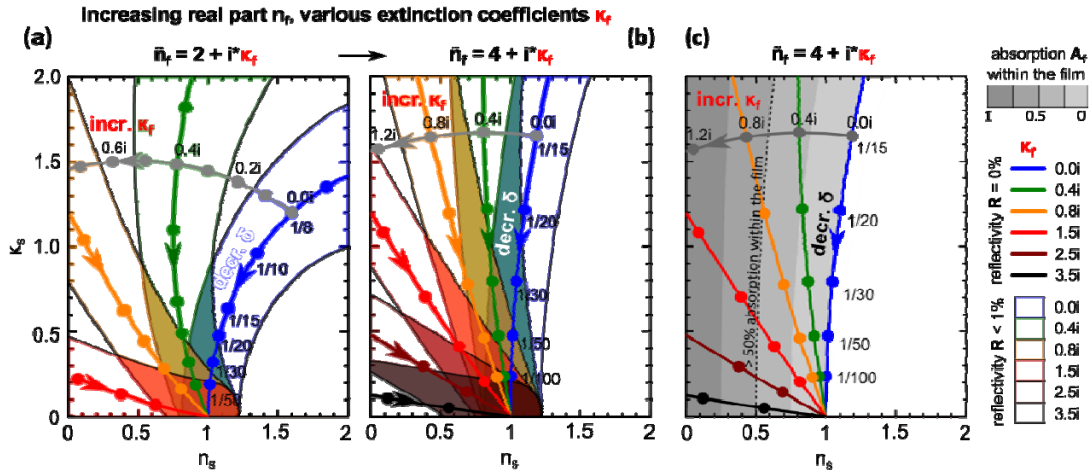

FIG. 1. The reflection of light at an interface between air and certain types of substrate can be completely suppressed by applying a suitable, optically ultra-thin coating to the surface. The stack can be treated as an asymmetric Fabry-Perot cavity comprising a uniform thin film with thickness d and refractive index $\tilde{n}_f = n_f + i\kappa_f$, sandwiched between air ($\tilde{n}_0 = 1$) and a substrate with refractive index $\tilde{n}_s = n_s + i\kappa_s$ (inset in A). (I-III**)** and (III-V) Maps of the calculated reflectance R as a function of n_s and κ_s for various κ_f and reduced thicknesses of the film $\delta = (d\, n_f)/\lambda$, respectively. A point of zero reflection (marked as colored dots in I-V) occurs for one particular combination of n_s, κ_s. (A) For a given complex refractive index of the film, the point of zero reflection follows an index trajectory $\tilde{n}_s(\delta)$ (blue line). A similar index trajectory $\tilde{n}_s(\kappa_f)$ (red line) results for a constant reduced thickness δ of the film.

Defining $\delta = d n_f / \lambda$ as a reduced thickness (notice, n_f is the real part of the film index), a reflection map can be calculated as a function of real (n_s) and imaginary (κ_s) parts of the substrate index by keeping n_f, κ_f and δ constant [Figs. 1(I-V)]. Fig. 1(III) shows the reflection map for a film with $\tilde{n}_f = 2 + 0.2i$ and $\delta = 1/8$. A point of zero reflection occurs for one particular combination of n_s and κ_s – in this case at $\tilde{n}_s \sim 1.21 + 1.38i$ (black dot). Since such a substrate is opaque and no light is reflected, the incident light is completely absorbed. For all other combinations of n_s and κ_s, light is partially reflected. By decreasing δ while keeping the refractive index of the film constant [Figs. 1(III-V)], the point of zero reflection moves in n_s-κ_s parameter space along a curved index trajectory $\tilde{n}_s(\delta)$ toward $\tilde{n}_s = 1 + 0i$ [Fig. 1(A) – blue

line]. Similarly, an index trajectory $\tilde{n}_s(\kappa_f)$ for zero reflection is obtained for a constant reduced thickness of the film, for instance $\delta = 1/8$, by increasing the extinction coefficient κ_f while keeping n_f constant [Figs. 1(I-III), 1(A) – red line].

Figs. 2(a) and 2(b) summarize combinations of specific film/substrate refractive indices and reduced film thicknesses that result in suppression of reflectance. Colored lines indicate the point of zero reflectance in n_s-κ_s space $\tilde{n}_s(\delta)$ as a function of δ, for a given film refractive index $\tilde{n}_f$. Grey lines illustrate the κ_f dependence of the point of zero reflectance $\tilde{n}_s(\kappa_f)$ for a given δ. The colored semi-transparent areas indicate the complex refractive index region of the substrate for which the reflectivity is smaller than 1%.
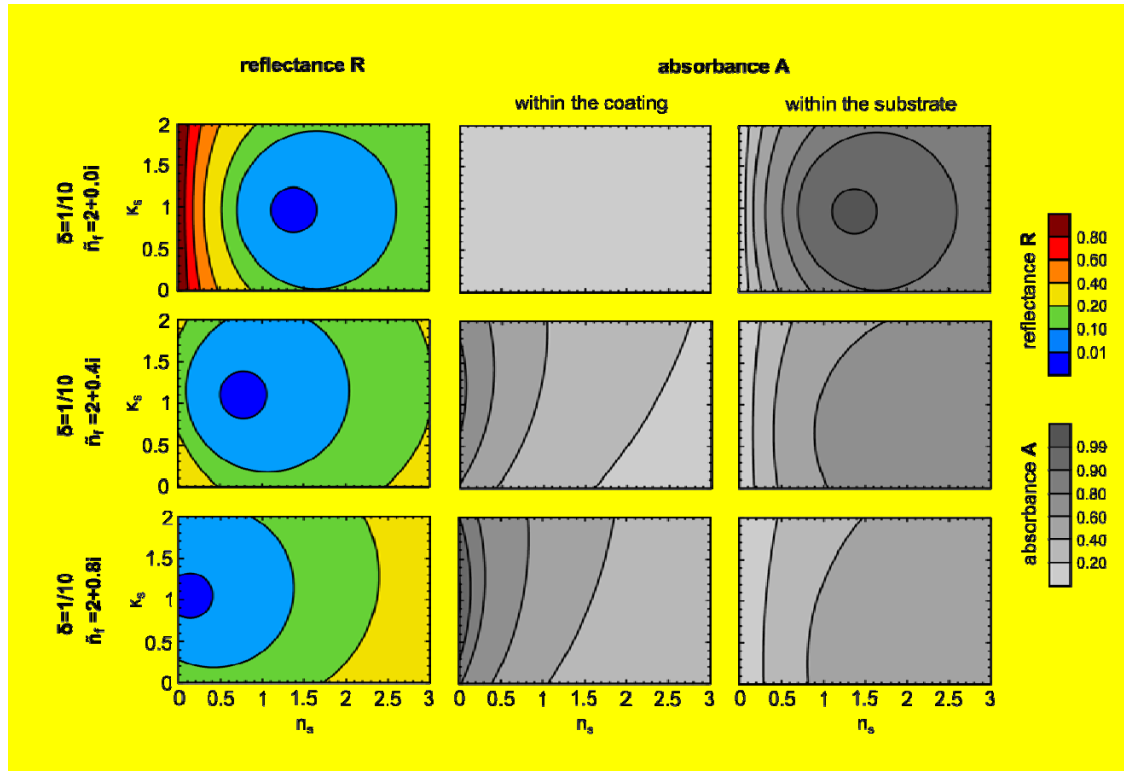

FIG. 2. General strategy to suppress reflection using ultra-thin coatings. (a, b) Zero reflection index trajectories $\tilde{n}_s(\delta)$ as a function of reduced film thickness $\delta = d/\lambda$ for various extinction coefficients κ_f of the film. The corresponding colored semi-transparent region indicates the refractive index region for which the reflectivity is smaller than 1%. Index trajectories are shown for $n_f = 2$ (a) and $n_f = 4$ (b), respectively. Zero reflection can only occur for films with $0 \leq \kappa_f < n_f$ and suitable δ. For ultra-thin films ($d \ll \lambda$), zero reflection almost exclusively occurs on substrates with _____ and small optical losses $0 < \kappa_s$ 2. (c) Index trajectories of the point of zero reflection (compare a) and greyscale-map of the amount of absorbed light A_{film} within the film.

Thus, from Figs. 2(a) and 2(b) the appropriate optical constants and thickness for the substrate and film can be read off for suppressing reflectance for a given wavelength. Note, that zero reflection can be only achieved using films with $\kappa_f < n_f$. The reflectance is not very sensitive to small changes of the refractive indices of either the film or the substrate [colored semi-transparent areas in Figs. 2(a),(b)], and has only a weak dependence on the angle of incidence for small angles $< 30°$ [36, 39, 59].

In a cavity comprising an ultra-thin film coating on a substrate, perfect *total* absorption is the complete absorption of light within the film and substrate. This is easily achieved on opaque

substrates when the coating leads to a complete suppression of reflected light. Note that perfect *total* absorption is different from perfect absorption within the film or within the substrate. Fig. 2(c) shows, in grayscale, the amount of absorbed light within the film (A_f) at the point of zero-reflection for $\tilde{n}_f = 4 + i\kappa_f$. Since no light is reflected, $A_s = 1 - A_f$ is the amount of light absorbed in the substrate.

In a cavity comprising an ultra-thin film coating on a substrate, perfect *total* absorption is the complete absorption of light within the film and substrate. Perfect *total* absorption is easily reached on opaque substrates when the coating leads to a complete suppression of reflected light. Perfect *total* absorption is different from perfect absorption within the film or perfect absorption within the substrate.

Figure 3: Maps of the calculated reflectance R, absorbance within the film, and absorbance within the substrate, of the cavity with $\tilde{n}_f = 2+0.0i$, $\tilde{n}_f = 2+0.4i$, and $\tilde{n}_f = 2+0.8i$ as a function of the real   and imaginary part   of the refractive index of the substrate. The reduced thickness of the film was fixed to $\delta = 1/10$.

Figure 3 summarizes three different scenarios: First, if the film is transparent: $\kappa_f = 0$, no light is absorbed within the coating. Thus, the point of zero reflectance in n_s-κ_s space is the same like the point of unity absorption within the opaque substrate. Perfect *total* absorption and perfect absorption within the substrate is the same. Secondly, if the film is lossy: $\kappa_f > 0$, but the point of zero reflectance is found at $n_s > 0$, it is neither possible to reach perfect absorption

In summary, especially Fig. 2 demonstrates that completely suppressed reflection, and thus near-perfect absorption, for near-normal incidence using optically ultra-thin coatings ($\delta << 1/4$) almost exclusively occurs on substrates with $n_s \lesssim 1$. Furthermore, low-loss substrates are needed to minimize the film thickness for which light reflection is completely suppressed. In particular, this is the reason why metals are impractical as substrate materials beyond the visible. Although they are low index materials, they are also highly lossy in the mid-infrared and suitable AR coatings become very thick.

B. Substrate materials with n < 1

Low-loss noble metals, e.g. Ag and Au, highly doped semiconductors, especially oxide semiconductors like aluminum doped ZnO (AZO), and polar dielectrics (e.g. SiO$_2$), behave like ENZ materials near their plasma frequencies or phonon resonance frequencies. At these frequencies n becomes significantly smaller than unity, provided the material is low-loss near the ENZ condition. The optical properties of those materials can be described using a Drude (complex permittivity ε_D) or Lorentz oscillator model (ε_L), respectively[60]:
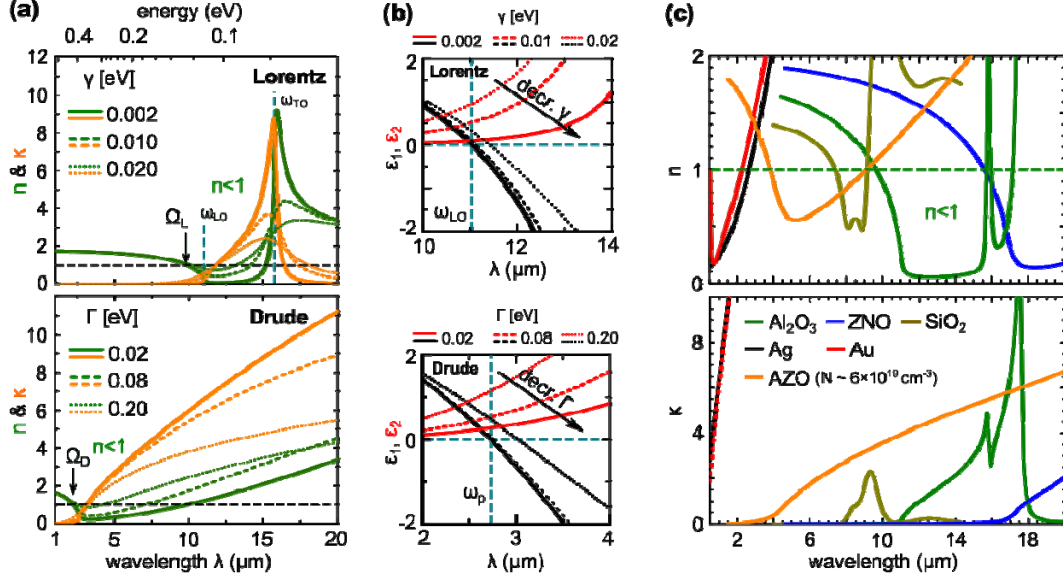
$$\epsilon_D = \epsilon_\infty \left(1 - \frac{\omega_p^2}{\omega(\omega + i\Gamma)}\right), \qquad \epsilon_L = \epsilon_\infty \left(1 + \frac{\omega_{LO}^2 - \omega_{TO}^2}{\omega_{TO}^2 - \omega^2 - i\omega\gamma}\right). \qquad (2)$$

Here, ε_∞ is the background permittivity, ω_p is the screened plasma frequency, which is proportional to the free-carrier concentration N: $\omega_p^2 = Ne^2/(\epsilon_0\epsilon_\infty m^\star)$, where e is the elementary charge, ε_0 is the vacuum permittivity, and m^* is the effective mass. Γ is a damping factor associated with the mobility of the charge carriers μ: $\Gamma \propto \mu^{-1}$. In the Lorentz oscillator model ω_{LO} and ω_{TO} are the longitudinal optical (LO) and transverse optical (TO) phonon frequencies, respectively, and the damping factor γ is related to the phonon lifetime τ: $\gamma \propto \tau^{-1}$.

A phonon resonance can be described by a single Lorentz oscillator as shown in Fig. 4(a) for a polar dielectric material with different values of γ. The coherent oscillation of vibrating bound charges on the atomic lattice of these materials results in a negative permittivity between ω_{LO} and ω_{TO} with an ENZ condition ($\varepsilon_I = 0$) close to ω_{LO} [Fig. 4(b)]. This spectral

region of negative permittivity is called the Reststrahlen band, and is characterized by $\kappa > n$, indicating that the insulating material has "metal-like" optical properties in this interval, such as a large reflectance coefficient when light is incident on the material from air. Values of n ≤ 1 can be found provided $\gamma << \omega_{TO}$ (low optical losses) within and just before the Reststrahlen region, starting at: $\Omega_L^2 \sim \left(\omega_{TO}^2 - \epsilon_\infty \omega_{LO}^2\right)(\epsilon_\infty - 1)^{-1}$. Low optical losses in polar materials are the result of the slow scattering rates of optical phonons, which typically occur on the timescale of picoseconds compared to the faster scattering rate of free-charge-carrier plasmons in highly doped semiconductors[54, 61]. Thus, very low n values can be reached [e.g., Al_2O_3 and ZnO in Figure 4(c)]. According to our strategy Fig. 2, suppression of reflection can be achieved with a suitable combination of an ultra-thin film and a polar substrate material, at a wavelength that corresponds to a Reststrahlen band of the substrate[31, 39, 45]. However, the feasibility of this approach is limited by the supply of suitable Reststrahlen materials[61] that determine the wavelength at which suppressed reflection and near-perfect absorption can be realized.

In metals, doped semiconductors, and conducting oxides, the contribution of free carriers to the optical properties can be described by the Drude model, shown in Fig. 4(a) for different values of Γ. Optical properties typically consistent with metals, $\kappa > n$, are found at wavelengths larger than the crossover wavelength at which $\varepsilon_1 = 0$. Especially for high carrier mobilities (weakly damped systems, $\Gamma << \omega_p$), characteristically low n values of ≤ 1 can be found in the vicinity of the crossover wavelength starting at $\Omega_D^2 \sim \epsilon_\infty \omega_p(\epsilon_\infty - 1)^{-1}$. Especially when the mobility increases (Γ decreases), losses (ε_2) are reduced, and small values of n can be reached [compare Fig. 4(b)].

FIG. 4. Epsilon near-zero substrate materials. (a) Lorentz oscillator model for polar dielectric materials and Drude model refractive indices n and κ for various damping constants γ and Γ, respectively. The model parameter values are: $\omega_p = 0.46$ eV, $\varepsilon_\infty = 5$, $\omega_{TO} = 0.079$ eV, $\omega_{LO} = 0.112$ eV. (b) Real ε_1 and imaginary part ε_2 of the dielectric function in the vicinity of the cross-over wavelength ($\varepsilon_1 = 0$). (a, b) For both models, n becomes vanishingly small at $\varepsilon_1 \sim 0$ provided the material is low-loss; that is small γ, Γ, respectively. Metal-like optical properties with $\kappa > n$ are found for wavelength larger than the cross-over wavelength whereas the region of $n < 1$ already starts at $\Omega_{D,L}$. (c) Real and imaginary parts, n and κ, of the refractive index of Ag [63], Au [63], SiO$_2$ [64], Al$_2$O$_3$, ZnO and AZO (N $\sim 6 \times 10^{19}$ cm^{-3}). In contrast to the metals, κ of SiO$_2$, Al$_2$O$_3$, ZnO and AZO is rather small in the spectral region where n < 1. AZO features a spectral region with n < 1 in the mid-infrared that depends on the free carrier concentration, whereas ZnO is transparent with n > 1 up to 16 μm.

In conventional metals, N is very large ($N \sim 10^{23}$ cm^{-3}), and the plasma resonance is usually located in the visible or ultraviolet[62]. The region of $n < 1$ extends far beyond the visible in metals such as Au and Ag, because ε_1 is negative and $|\varepsilon_1| \gg \varepsilon_2$. Although they are ideal substrates for the visible range[32, 38], they cannot be used as substrate materials for *ultra-thin* coatings to achieve completely suppressed reflection at longer wavelengths, such as the near- and mid-infrared, because $\kappa \gg 1$ [see Figs. 2(a), (b) and 4(c)].

The limitations of metals can be circumvented by modifying the free-carrier concentration in semiconductors through impurity doping[65]. The maximum free carrier concentration that can be achieved by doping is an intrinsic property of each semiconductor, determined by the location of the semiconductor band edges with respect to the Fermi level stabilization energy[66]. In most semiconductors, the achievable free-carrier concentration is orders of

magnitude smaller compared to that of metals due to solid-solubility limits and charge compensation. However, oxide semiconductors such as ZnO, can be heavily doped, e.g. with aluminum, without significant alteration of their structural properties[67], e.g. phase separation, reaching carrier concentrations of the order of $N \sim 10^{21}$ cm^{-3} [53, 54], which establishes plasma resonances in the near- and mid-infrared. Furthermore, the plasma frequency in these materials is widely tunable by adjusting the doping density. Low-loss oxide semiconductors are thus a versatile substrate platform for suppressed reflection and near-perfect absorption in the spectral gap between the visible and the infrared.
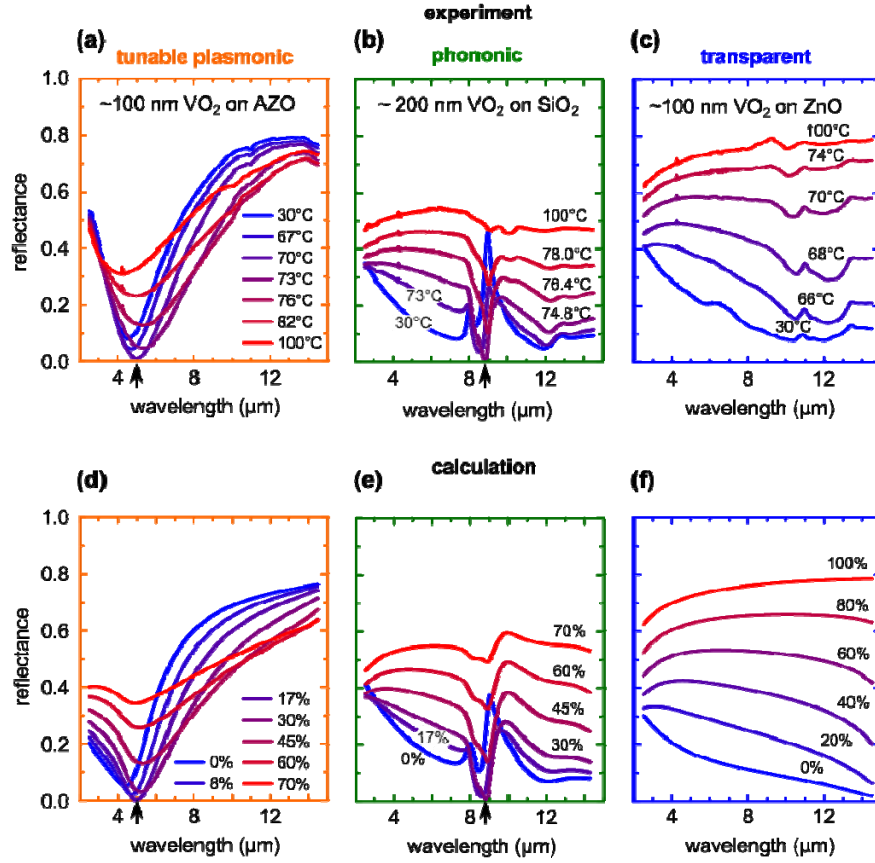
C. Experimental verification

The optical properties of our AZO substrate ($c_{Al} \sim 1 \times 10^{20}$ cm^{-3}), as determined by spectroscopic ellipsometry, are shown in yellow in Fig. 4(c). The free-carrier concentration was found to be $N \sim 6 \times 10^{19}$ cm^{-3} in this particular sample. "Metal-like" optical properties ($\kappa > n$) can be observed above the crossover wavelength $\lambda \sim 4.4$ µm, and the spectral region of $n < 1$ ranges from 3.7 to 9.2 µm. Crossover wavelengths as small as $\lambda \sim 1.3$ µm have been reported for highly doped ZnO[54]. Thus, AZO is a suitable plasmonic substrate in the spectral gap between the visible and the infrared.

Figures 4a-c summarize the experimentally determined temperature-dependent reflectance of VO$_2$ films deposited on substrates that are dominated by a plasma resonance (AZO), feature prominent phonon resonances (SiO$_2$), or are transparent in the mid-infrared (ZnO). Figure 5(a) shows the temperature-dependent reflectance of a ~100 nm-thin ($\delta \sim 1/20$ at 5 µm) VO$_2$ film deposited on an AZO substrate ($N \sim 6 \times 10^{19}$ cm^{-3}). At low temperatures, when VO$_2$ is still insulating, the reflectance spectra are dominated by the onset of metallic reflectivity of the AZO substrate. Upon heating, in the vicinity of the phase transition of VO$_2$, a minimal reflectance value of $R_{min} = 0.01$ is reached at $\lambda_{min} = 5.0$ µm, which is close to the crossover wavelength of $\lambda = 4.4$ µm, and $T_{min} = 70$ °C. At this wavelength, the refractive index of the AZO is $n_s = 0.56 + 1.09i$, in agreement with our predictions (Figs. 1 and 2).

The reflectance of a 200 nm ($\delta \sim 1/19$ at $\lambda = 8.8$ µm, comparable to VO$_2$ on AZO) VO$_2$ film on SiO$_2$ shows a similar temperature-dependent behavior [Fig. 5(b)]. At low temperatures, the reflectance spectrum is dominated by the Reststrahlen band of SiO$_2$ that extends from 7.9 and 9.2 µm [64] [Fig. 4(c)]. Upon heating, the reflectance reaches a minimum $R_{min} = 0.005$ at

$\lambda_{min} = 8.8$ µm and $T_{min} = 73$ °C. At high temperatures, the reflectance is dominated by the reflectance of the VO$_2$ film in the metallic state. At the point of minimal reflection, the refractive index of the SiO$_2$ substrate is $\tilde{n}_3 = 0.47 + 1.19i$. A comparable reflectance minimum was found for ultra-thin VO$_2$ films ($\delta < 1/30$) on Al$_2$O$_3$ within the Reststrahlen band of the Al$_2$O$_3$ substrate that extends from ~11 to 15.8 µm [31, 45].

FIG. 5. Experimental demonstration of suppressed reflection in the vicinity of substrate phonon and plasmon resonances using ultra-thin coatings. (a-c) Measured temperature-dependent mid-IR reflectance cycle of ultra-thin (thickness $d << \lambda$) VO$_2$ grown on AZO with N ~ 6×10^{19} cm^{-3} (a), SiO$_2$ (b), and ZnO (c), respectively. All spectra are measured during a heating cycle. A reflectance minimum (marked with an arrow) occurs for VO$_2$ on the AZO substrate in the vicinity of the AZO plasma resonance. A comparable reflectance minimum is found in the Restrahlen band of the SiO$_2$ substrate that is bound by the LO and TO phonon between 7.9 and 9.2 µm [61]. No local minimum is observed for VO$_2$ on a ZnO substrate. (d-f) Calculated reflectance of the samples described in (a-d) as a function of the fraction of metallic phase in the VO$_2$ film.
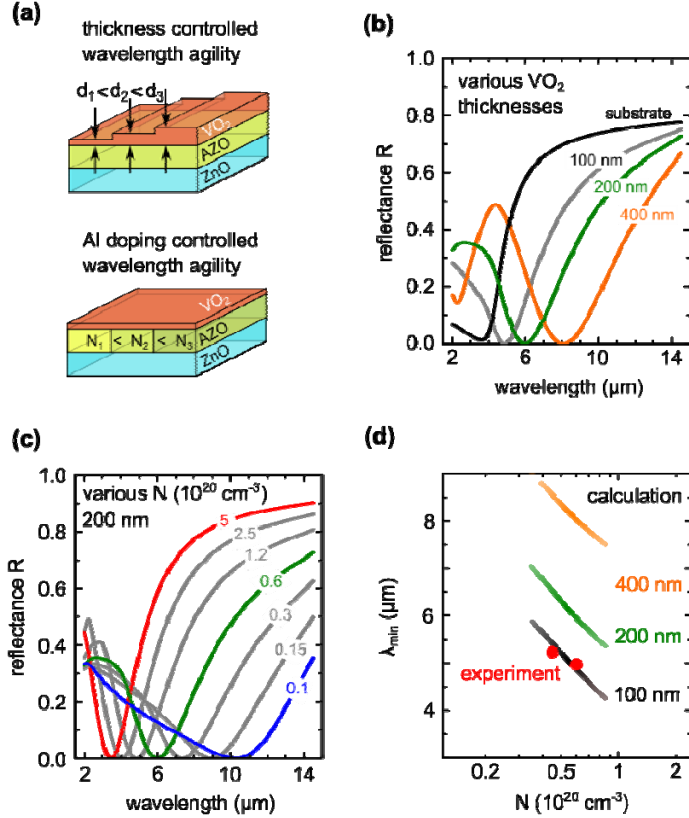
No reflectance minimum is observed for a 100 nm thin VO_2 film on ZnO, because the ZnO refractive index is $n > 1$ across the entire wavelength range [Figs. 5(c) and 4(c)]. The high-temperature reflectance of the VO_2 film grown on AZO and SiO_2 is significantly lower than for VO_2 grown on intrinsic ZnO [compare Figs. 5(a),(b) and 5(c)], which we attribute to a lower film quality of VO_2/AZO and VO_2/SiO_2, especially with many extended defects and void formation at the interface.

Figs. 5(d)-(f) show the calculated reflectance of an ultra-thin VO_2 film on AZO, SiO_2, and ZnO, respectively, as a function of the fraction of metallic phase within the VO_2 film. At room temperature, VO_2 is in the insulating state and the metallic fraction is zero, whereas at high temperatures VO_2 is entirely in the metallic state. For this purpose, the refractive index of VO_2 was estimated in the vicinity of the phase transition from experimental data obtained by spectroscopic ellipsometry[31, 44] and by effective medium approximation[44, 45]. Note, that the experimentally obtained refractive index data[31, 44, 45] were obtained for high quality VO_2 films grown on (001) Al_2O_3. In all cases, the calculated reflectance is in very good agreement with the experimental data. We do note, however, that the measured high-temperature reflectance VO_2 on AZO and SiO_2 [Figs. 5(a) and (b)] is in agreement with the calculations given a metallic fraction of ~70 %, instead of the expected 100 %. We attribute this discrepancy to a large amount of structural defects affecting the optical properties of VO_2. Further, the calculations underestimate the reflectance of the VO_2 films on AZO especially in the insulating state at short wavelength [2 – 4 μm, Figs. 5(a) and (d)]. This can be attributed to both, the quality of the VO_2 film and the assumption of a semi-infinite substrate made in equation (1). However, strong interference effects within the AZO layer, which would significantly affect the reflectance, are not supposed, due to the Gaussian doping tail.

D. Wavelength tenability

Calculations summarized in Fig. 6 show that for ultra-thin VO_2 films on an AZO substrate, the wavelength of minimal reflection λ_{min} can be tuned over a broad range either by changing the thickness of the VO_2 film [Figs. 6(a), (b)], or by changing the free-carrier concentration N of the AZO substrate [Figs. 6(a), (c)]. Note that all reflectance spectra are given for a metallic fraction of the VO_2 film at which the reflectance is the smallest. Increasing the VO_2 film thickness from 100 to 400 nm and keeping $N \sim 6 \times 10^{20}$ cm^{-3} of the AZO constant, λ_{min} shifts from 5 to ~ 8 μm [Figs. 6(b), (d)]. Maintaining the film thickness constant at 200 nm and changing N between 0.1 and 5×10^{20} cm^{-3}, accessible by impurity doping[51, 53, 54], results in the

tuning of the minimum reflection point from ~10.5 to ~3.5 μm [Figs. 5(c), (d)]. Our experimental results are in good agreement with the calculations, resulting in λ_{min} = 5.0 and 5.3 μm for 100 nm VO$_2$ films on AZO substrates with $N \sim$ 0.45 and 0.6× 10^{20} cm^{-3} (Figs. 5(a), 6(d)], respectively. Our results show that, depending on the VO$_2$ film thickness and the doping concentration, the wavelength of minimal reflection can be precisely tuned between the phonon resonance of intrinsic ZnO and the highest plasma wavelength achievable in doped ZnO.

FIG. 6. (a) Wavelength agility of the point of zero reflection can be achieved by varying the VO$_2$ film thickness or by changing the Al dopant concentration of the AZO substrate. (b) Calculated reflectance of thin VO$_2$ films on AZO ($N \sim 6 \times 10^{19}$ cm^{-3}) for different VO$_2$ film thicknesses. The wavelength of minimal reflectance λ_{min} increases with increasing film thickness. (c) Calculated reflectance of a 200 nm VO$_2$ film on AZO for different free-carrier concentrations N. λ_{min} decreases with increasing N (d) Comparison of the experimental and calculated λ_{min}.

IV. Conclusions

In summary, we introduced a methodical strategy to design highly absorbing anti-reflection coatings comprising ultra-thin films on opaque substrates. The reflection of light can be completely suppressed using a suitable film/substrate combination, if the refractive index of the substrate is n ≲ 1, thus close to the epsilon-near-zero condition. We demonstrated both
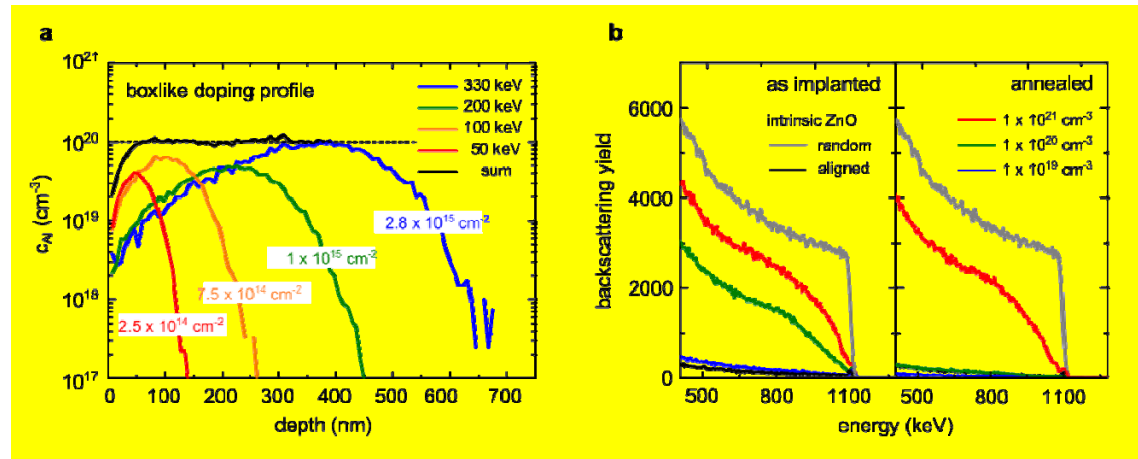
theoretically and experimentally that this condition can be achieved over a wide range of wavelengths by using semiconductors with widely tunable carrier densities, such as aluminum-doped zinc oxide (AZO). We experimentally verified this approach by using an ultra-thin film of vanadium dioxide on an AZO substrate. In this system, the wavelength at which minimal reflection occurs can be tuned over the entire mid-infrared range by changing the free-carrier concentration of the AZO substrate. We anticipate that the development of new low-loss epsilon-near-zero substrates in the near- and mid-infrared will enable efficient single layer ultra-thin absorbers for photodetection and thermal emission applications.

Acknowledgements

Appendix: Ion beam aluminum doped zinc oxide

Aluminum (Al) doped ZnO substrates (AZO) with various doping concentrations were prepared by multiple energy Al ion implantation of (001) ZnO. Figure 7(a) shows the individual concentration depth profiles calculated for various energies using the SRIM code[68] and the sum profile. Ion fluences are indicated for a doping concentration of $c_{Al} \sim 1 \times 10^{20}$ cm^{-3}. The sum doping profile consists of a 400 nm thick layer with nearly constant Al concentration and a Gaussian tail that extends additional ~ 200 nm into the substrate.

Figure 7: **a** A boxlike doping profile of Al dopants in ZnO was achieved by multiple energy and fluence ion implantation. **b** Rutherford backscattering spectrometry with 1.4 He$^+$ ions in channeling direction of as implanted and annealed AZO samples for various aluminum dopant concentrations. The aligned and random spectra of intrinsic ZnO are given for comparison.

The high implantation temperature and subsequent annealing at 700°C for one hour in air was necessary to maintain high crystallinity. The crystal quality after irradiation and after annealing was determined via 1.4 MeV He$^+$ Rutherford backscattering spectrometry in channeling configuration. For the implantation and annealing conditions used, a high crystalline quality (low backscattering yield in channeling direction) was observed at nominal dopant concentration as high as $c_{Al} \sim 1\times10^{20}$ cm^{-3}, as shown in figure 7b.

The effective optical properties of the AZO substrate doped with a nominal aluminium concentration of $c_{Al} \sim 1\text{x}10^{20}$ cm^{-3} are well described by a dielectric function consisting of two terms: a single Lorentzian oszillator taking into account the phonon resonance, and a Drude term that describes the free-electron contribution caused by Al$^+$ doping:

$$\epsilon(\omega) = \epsilon_\infty \left(1 + \frac{\omega_{LO}^2 - \omega_{TO}^2}{\omega_{TO}^2 - \omega^2 - i\omega\gamma} - \frac{\omega_p^2}{\omega(\omega + i\Gamma)} \right) = \epsilon_\infty + \frac{f\omega_o^2}{\omega_o^2 - \omega^2 - i\gamma\omega} - \frac{\epsilon_\infty \omega_p^2}{\omega(\omega + i\Gamma)}, \qquad \text{(I)}$$

where ε_∞ = 3.65 is the high energy dielectric constant, f = 3.98 is the phonon oscillator strength, ω_0 = 0.051 eV, is the phonon resonance energy, w_p = 0.28 eV the screened plasma energy, corresponding to a crossover wavelength of $\lambda_p \sim 4.4$ µm, and γ = 0.0019 eV, Γ = 0.071 eV are the damping factors related to energy dissipation e.g. by scattering processes.

Al$^+$ ion beam doping to a nominal doping concentration of $c_{Al} \sim 1\text{x}10^{20}$ cm^{-3} and subsequent annealing at 700°C in air for 1h leads to a free-carrier concentration $N \sim 0.6 \times c_{Al} \sim 6\times10^{19}$ cm^{-3} in this particular sample. The AZO layer is basically transparent in the visible and near-IR spectral range, but possess metal-like optical properties ($\kappa_s > n_s$) above $\lambda_p \sim 4.4$ µm. However, $n_s < 1$ with increasing κ_s from 0.3 to 3.2 is found in the spectral range from 3.7 to 9.2 µm (compare figure 4c).

References

1   T. Tiedje, E. Yablonovitch, G. D. Cody, and B. G. Brooks, *Limiting efficiency of silicon solar cells,* IEEE Trans. Electron Dev. **31**, 711–716 (1984).

2   L. Hu, and G. Chen, *Analysis of Optical Absorption in Silicon Nanowire Arrays for Photovoltaic Applications,* Nano Lett. **7**, 3249-3252 (2007).

3   Y. M. Song, J. S. Yu, and Y. T. Lee, *Antireflective submicrometer gratings on thin-film silicon solar cells for light-absorption enhancement.* Opt. Lett. **35**, 276-278 (2010).

4   M. Bernardi, M. Palummo, and J. C. Grossman, *Extraordinary Sunlight Absorption and One Nanometer Thick Photovoltaics Using Two-Dimensional Monolayer Materials,* Nano Lett. **13**, 3664-3670 (2013).

5   A. Polman, M. Knight, E. C. Garnett, B. Ehrler, and W. C. Sinke, *Photovoltaic materials: Present efficiencies and future challenges.* Science **352**, aad4424 (2016).

6   D. Rodrigo, O. Limaj, D. Janner, D. Etezadi, F. J. Garcia de Abajo, V. Pruneri, and H. Altug, *Mid-infrared plasmonic biosensing with graphene.* Science **349**, 165-168 (2015).

7   M. W. Knight, H. Sobhani, P. Nordlander, and N. J. Halas, *Photodetection with Active Optical Antennas.* Science **332**, 702-704 (2011).

8   N. Liu, M. Mesch, T. Weiss, M. Hentschel, and H. Giessen, *Infrared Perfect Absorber and Its Application As Plasmonic Sensor.* **10**, 2342-2348 (2010).

9   J. A. Mason, S. Smith, and D. Wasserman, *Strong absorption and selective thermal emission from a midinfrared metamaterial.* Appl. Phys. Lett. **98**, 241105 (2011).

10   J. M. LLoyd. *Thermal imaging systems*: (Springer Science & Business Media, 2013).

11   J. A. Schuller, T. Taubner, and M. L. Brongersma, *Optical antenna thermal emitters.* Nat. Photon. **3**, 658-661 (2009).

12   M. A. Kats, R. Blanchard, S. Zhang, P. Genevet, C. Ko, S. Ramanathan, and F. Capasso, *Vanadium Dioxide as a natural disordered metamaterial: perfect thermal emission and large broadband negative differential thermal emittance,* Phys. Rev. X **3**, 041004 (2013).

13   W. Streyer, S. Law, G. Rooney, T. Jacobs, and D. Wasserman. *Strong absorption and selective emission from engineered metals with dielectric coatings*, Opt. Express **21**, 9113-9122 (2013).

14   C. Argyropoulos, K. Q. Le, N. Mattiucci, G. D'Aguanno, and A Alù, *Broadband absorbers and selective emitters based on plasmonic Brewster metasurface*, Phys. Rev. B **87**, 205112 (2013).

15   H. K. Raut, V. A. Ganesh, S. A. Nair, and S. Ramakrishna, *Anti-reflective coatings: A critical, in-depth review*, Energy Environ. Sci. **4**, 3779-3804 (2011).

16   M. J. Minot. *Single-layer, gradient refractive index antireflection films effective from 0.35 μm to 2.5 μm*, J. Opt. Soc. Am. **66**, 515-519 (1976).

17   J.-Q. Xi, M. F. Schubert, J. K. Kim, E. F. Schubert, M. Chen, and S.-Y. Lin, *Optical thin-film materials with low refractive index for broadband elimination of Fresnel reflection*, Nat. Photon. **1**, 176-179 (2007).

18   J. Hao, J. Wang, X. Liu, W. J. Padilla, L. Zhou, and M. Qiu, *High performance optical absorber based on a plasmonic metamaterial*, Appl. Phys. Lett. **96**, 251104 (2010).

19   X. Liu, T. Tyler, T. Starr, A. F. Starr, N. M Jokerst, and W. Padilla, *Taming the Blackbody with Infrared Metamaterials as Selectrive Thermal Emitters*, Phys. Rev. Lett. **96**, 251104 (2010).

20   H.-T. Chen, *Interference theory of metamaterial perfect absorbers*, Opt. Express **7**, 7165-7172 (2012).

21   X. Shen, Y. Yang, Y. Zang, J. Gu, J. Han, W. Zhang, and T. Cui, *Triple-band terahertz metamaterial absorber: Design, experiment, and physical interpretation*, Appl. Phys. Lett. **101**, 154102 (2012).

22   A. Kabiri, E. Girgis, and F. Capasso, *Buried Nanoantenna Arrays: Versatile Antireflection Coating*, Nano Lett. **13**, 6040-6047 (2013).

23   Y. Cui, Y. He, Y. Jin, F. Ding, L. Yang, Y. Ye, S. Zhong, Y. Lin, and S. He, *Plasmonic and metamaterial structures as electromagnetic absorbers*, Laser Photon. Rev. **8**, 495-520 (2014).

24   Y. Yao, R. Shankar, M. A. Kats, Y. Song, J. Kong, M. Loncar, and F. Capasso, *Electrically tunable metasurface perfect absorber for ultrathin mid-Infrared optical modulators*, **14**, 6526-6532 (2014).

25   K. Liu, X. Zeng, S. Jiang, D. Ji, H. Song, N. Zhang, and Q. Gan, *A large-scale lithography-free metasurface with spectrally tunable super absorption.* Nanoscale **6**, 5599-5605 (2014).

26 R. F. Waters, P. A. Hobson, K. F. MacDonald, and N. I. Zheludev, *Optically switchable photonic metasurfaces*, Appl. Phys. Lett. **107**, 081102 (2015).

27 L. Cong, S. Tan, R. Yahiaoui, F. Yan, W. Zhang, and R. Singh, *Experimental demonstration of ultrasensitive sensing with terahertz metamaterial absorbers: A comparison with the metasurface*, Appl. Phys. Lett. **106**, 031107 (2015).

28 W. Dong, Y. Qiu, J. Yang, R. E. Simpson, and T. Cao, *Wideband Absorbers in the Visible with Ultrathin Plasmonic-Phase Change Material Nanogratings*, J. Phys. Chem. C. **120**, 12713-12722 (2016).

29 H.A. Haus, *Waves and Fields in Optoelectronics* (Englewood Cliffs, NJ: Prentice-Hall 1984).

30 A. Yariv, *Critical Coupling and Its Control in Optical Waveguide-Ring Resonator Systems*, IEEE Photon. Technol. Lett. **14**, 483-485 (2002).

31 M. A. Kats, D. Shama, J. Lin, P. Genevet, R. Blanchard, Z. Yang, M. M. Qazilbash, D. N. Basov, S. Ramanathan, and F. Capasso, *Ultra-thin perfect absorber employing a tunable phase change material*, Appl. Phys. Lett. **14**, 483-485 (2012).

32 M. A. Kats, R. Blanchard, P. Genevet, and F. Capasso, *Nanometre optical coatings based on strong interference effects in highly absorbing media*, Nat. Mater. **14**, 483-485 (2013).

33 F. F. Schlich, and R. Spolenak, *Strong interference in ultrathin semiconducting layers on a wide variety of substrate materials*. Appl. Phys. Lett. **103**, 213112 (2013).

34 J. W. Cleary, R. Soref, and J. R. Hendrickson, *Long-wave infrared tunable thin-film perfect absorber utilizing highly doped silicon-on-sapphire*. **21**, 19363-19374 (2013).

35 J. Park, J.-H. Kang, A. P. Vasudec, D. T. Schoen, H. Kim, H. Hasman, and M. L. Brongersma, *Omnidirectional Near-Unity Absorption in an Ultrathin Planar Semiconductor Layer on a Metal Substrate*, ACS Photonics **1**, 812-821 (2014).

36 K.-T. Lee, S. Seo, J. Y. Lee, and L. J. Guo, *Strong resonance effect in a lossy medium-based optical cavity for angle robust spectrum filters*, Adv. Mater. **1**, 812-821 (2014).

37 H. Kocer, S. Butun, Z. Li, and K. Aydin, *Reduced near-infrared absorption using ultra-thin lossy metals in Fabry-Perot cavities*, Sci. Rep. **5**, 8157 (2015).

38 J. Liang, L. Hou, and J. Li, *Frequency tunable perfect absorber in the visible and near-infrared regimes based on VO$_2$ phase transition using planar layered thin films*, J. Opt. Soc. Am. **33**, 1075-1080 (2016).

39 M. A. Kats, and F. Capasso, *Optical absorbers based on strong interference in ultra-thin films*, Laser Photon. Rev. **10**, 735-749 (2016).

40 I. Liberal, and N. Engheta, *Near-zero refractive index photonics*. Nat. Photon. **355**, 1058-1062 (2017).

41 H. Lim, N. Stavrias, B. C. Johnson, R. E. Marvel, R. F. Haglund Jr., and J. C. McCallum, *Optical switching and photoluminescence in erbium-implanted vanadium dioxide thin films*, J. Appl. Phys. **115**, 093107 (2014).

42 M. D. Goldflam *et al.*, *Voltage switching of a VO$_2$ memory metasurfaec using ionic gel*, Appl. Phys. Lett. **105**, 041117 (2014).

43 P. Markov, R. E. Marvel, H. J. Conley, K. J. Miller, R. F. Haglund Jr., and M. Sharon, *Optically monitored electrical switching in VO$_2$*, ACS Photon. **2**, 1175-1182 (2015).

44 M. M. Qazilbash *et al.*, *Mott transition in VO$_2$ revealed by infrared spectroscopy and nano-imaging*, Science **318**, 1750-1753 (2007).

45 J. Rensberg *et al.*, *Active optical metasurfaces based on defect-engineered phase-transition materials*, Nano Lett. **16**, 1050-1055 (2016).

46 D. S. Ginley, and C. Bright, *Transparent Conducting Oxides*, MRS Bull. **25**, 15-18 (2000).

47 B. G. Lewis, and D. C. Paine, *Applications and processing of transparent conducting oxides*, MRS Bull. **25**, 22-27 (2000).

48 E. Fortunato, D. Ginley, H. Hosono, and D. C. Paine, *Transparent conducting oxides for photovoltaics*, MRS Bull. **32**, 242–247 (2007).

49 A. Boltasseva, and H. A. Atwater, *Low-Loss Plasmonic Metamaterials*, Science **331**, 290-291 (2011).

50 G. V. Naik, J. Kim, and A. Boltasseva, *Oxides and nitrides as alternative plasmonic materials in the optical range*, Opt. Mater. Express **1**, 1090-1099 (2011).

51 G. V. Naik, J. J. Liu, A. V. Kildishev, V. M. Shalaev, and A. Boltasseva, *Demonstration of Al:ZnO as a plasmonic component for near-infrared metamaterials*, Proc. Natl. Acad. Sci. USA **109**, 8834-8838 (2012).

52 M.-C. Jun, S.-U. Park, and J.-H. Koh, *Comparative studies of Al-doped ZnO and Ga-doped ZnO transparent conducting oxide thin tilms*, Nanoscale Res. Lett. **7**, 639 (2012).

53 K. Ellmer, *Past achievments and future challenges in the development of optically transparent electrodes*, Nat. Photon. **6**, 809-817 (2012).

54 J. Kim *et al.*, *Role of epsilon-near-zero substrate in the optical response of plasmonic antennas*, Optica **3**, 339-346 (2016).

55 Z. Q. Chen, M. Maekawa, S. Yamamoto, A. Kawasuso, X. L. Yuan, T. Sekiguchi, R. Suzuki, and T. Ohdaira, *Evolution of voids on Al^+-implanted ZnO probed by a slow positron beam*, Phys. Rev. B **69**, 035210 (2004).

56 T. Borseth, J. S. Christensen, K. Maknys, A. Hallen, B. G. Svensson, and A. Y. Kuznetsov, *Annealing study of Sb^+ and Al^+ ion-implanted ZnO*, Superlattices Microstruct. **38**, 464-471 (2005).

57 F. J. Wong, Y. Zhou, and S. Ramanathan, *Epitaxial variants of VO_2 thin films on complex oxide single crystal substrates with 3m surface symmetry*, J. Cryst. Growth **364**, 74-80 (2013).

58 M. Born, and E. Wolf, *Principles of optics: electromagnetic theory of propagation, interference and diffraction of light* (Elsevier, 1980).

59 K.-T. Lee, S. Seo, J. Y. Lee, and L. J. Guo, *Ultrathin metal-semiconductor-metal resonator for angle invariant visible band transmission filters*, Appl. Phys. Lett. **104**, 231112 (2014).

60 P. Prunici, F. U. Hamelmann, W. Beyer, H. Kurz, and H. Stiebig. *Modelling of infrared optical constants for polycrystalline low pressure chemical vapour deposition ZnO:B films*, J. Appl. Phys. **113**, 123104 (2013).

61 J. D. Caldwell, L. Lindsay, V. Giannini, I. Vurgaftman, T. L. Reinecke, S. A. Maier, and O. J. Glembocki, *Low-loss, infrared and terahertz nanophotonics using surface phonon polaritons*, Nanophotonics **4**: 44-68 (2015).

62 M. A. Ordal, R. J. Bell, R. W. Alexander, L. L. Long, and M. R. Querry, *Optical properties of fourteen metals in the infrared and far infrared: Al, Co, Cu, Au, Fe, Pb, Mo, Ni, Pd, Pt, Ag, Ti, V, and W*, Appl. Opt. **24**, 4493-4499 (1985).

63 A. D. Rakic, A. B. Djurisic, J. M. Elazar, and M. L. Majewski, *Optical properties of metallic films for vertical-cavity optoelectronic devices*, Appl. Opt. **37**, 5271-5283 (1998).

64 J. Kischkat *et al.*, *Mid-infrared optical properties of thin films of aluminum oxide, titanium dioxide, silicon dioxide, aluminum nitride, and silicon nitride*, Appl. Opt. **51**, 6789-6798 (2012).

65 G. V. Naik, V. M. Shalaev, and A. Boltasseva, *Alternative plasmonic materials: beyond gold and silver*, Adv. Mater. **25**, 3264-3294 (2013).

66 W. Walukiewicz, *Intrinsic limitations to the doping of wide-gap semiconductors*, Physica B **302-303**, 123-134 (2001).

67 M. H. Yoon, S. H. Lee, H. L. Park, H. K. Kim, and M. S. Jang, *Solid solubility limits of Ga and Al in ZnO*. J. Mater. Sci. Lett. **21**, 1703-1704 (2002).

68 Biersack, J., Ziegler, J. *The Stopping and Ranges of Ions in Matter*. (Pergamon Press, Oxford, 1985).